

On Sensor Switching Visual Servoing

Kolja Kühnlenz and Martin Buss

Institute of Automatic Control Engineering (LSR)

Technische Universität München

D-80290 Munich, Germany

{kolja.kuehnlenz,mb}@ieee.org

phone: +49 89 2892 8396

Abstract

This article investigates dynamical camera switching during visual servoing tasks using multi-camera systems considering image-based and position-based Jacobian transpose control schemes. Stability is discussed using a common Lyapunov function assuming ideal target and camera models and multiple Lyapunov functions under parameter perturbations. It is shown that asymptotical stability cannot be achieved for arbitrary switching under parameter perturbations. Therefore, an energy supervised switching scheme is introduced guaranteeing asymptotical stability. The contribution are stable visual servoing strategies which facilitate instantaneous adjustments of control performance and dynamical device switches in case of task requirements or sensor breakdown.

keywords: computer vision, visual servoing, switched systems, hybrid systems, stability, robotics

Nomenclature

s	image features	σ	switching signal
K, K_v	gains	\mathcal{P}	index set
τ	torque	\mathcal{J}	set of Jacobians
J_i	image Jacobian	\mathcal{H}	set of sensors
J_t	robot Jacobian	f	vector field
h	sensor models	V	Lyapunov function
q	joint angles	$C_{i,j}$	equipotential lines
Z	distance in task-space	$(\cdot)_p, (\cdot)_q$	before and after a switch
e_i, e_t	control errors	t	time
g	gravity force	τ_i	time period
$(\cdot)^d$	desired value	Λ	perturbation matrix
$\hat{\cdot}$	estimated value	λ	focal-length
$C\dot{q}$	Coriolis-, centripetal torques	\bar{e}	average control error
M	inertia matrix	e_{pose}	control error trajectory
$W = [X Y Z \phi \theta \psi]^T$	relative pose in RPY	x_{pose}	trajectory
$\bar{W} = [X Y Z \phi_X \phi_Y \phi_Z]^T$	relative pose	σ_e	standard deviation

1 INTRODUCTION

Vision-based control of robot manipulators, commonly referred to as visual servoing, has been a research area of continued interest for more than three decades (Weiss et al. 1987; Feddema and Mitchell 1989; Espiau et al. 1992; K. Hashimoto, Ed. 1993; Papanikolopoulos et al. 1993; Martinet et al. 1996; Hutchinson et al. 1996; Wilson et al. 1996; Malis et al. 1999; Deguchi 1998; Corke and Hutchinson 2001). One or more cameras may either be fixed on the end-effector or in the environment and the control error may be defined in Cartesian as well as in image spaces resulting in various advantages and disadvantages (Hutchinson et al. 1996). So called partitioned approaches do also exist controlling different degrees of freedom of the robot manipulator in different spaces in order to overcome particular drawbacks of the conventional methods (Malis et al. 1999; Deguchi 1998; Corke and Hutchinson 2001). Some works on variable camera parameters exist (Hager 1995; Malis 2001), in particular, on zooming cameras (Hayman 2000; Hosoda et al. 1995; Malis and Benhimane 2003) in order to cope with field-of-view constraints and parameter dependent control performance. Only few works consider manipulator dynamics (Kelly et al. 2000; Deng et al. 2002). Recently, switched system approaches to visual servoing have been proposed which dynamically

switch between several control strategies (Gans and Hutchinson 2007; Hashimoto and Noritsugu 2000; Kühnlenz 2007; Kühnlenz and Buss 2007; Kühnlenz and Buss 2005; Mansard and Chaumette 2004). A few comprehensive review and taxonomy articles exist (Hutchinson et al. 1996; Kragic and Christensen 2002; Corke 1994). A substantial bibliography can also be found in (Chaumette et al. 2004).

Stability of conventional visual servoing has been proven in several works under different assumptions. Earlier works neglected dynamics and established basic stability conditions on the Jacobian (Espiau et al. 1992; Chaumette 1998; Malis et al. 1999; Weiss et al. 1987). Modern approaches account for nonlinear manipulator dynamics invoking Lyapunov's direct method in conjunction with Krasovskii-LaSalle's theorem proving (local) asymptotical stability (Kelly et al. 2000; Deng et al. 2002). Robustness has been analyzed in some works considering modeling uncertainties (Deng et al. 2002). More recent research is concerned with switched system stability (Hashimoto and Noritsugu 2000; Gans and Hutchinson 2007; Mansard and Chaumette 2004; Deng et al. 2005; Kühnlenz 2007), e.g. establishing a common Lyapunov function of the visual servoing subsystems (Gans and Hutchinson 2007; Kühnlenz 2007).

Recently we introduced a novel switching approach to visual servoing allowing dynamical switches of intrinsic and extrinsic camera parameters (Kühnlenz and Buss 2005; Kühnlenz 2007; Kühnlenz and Buss 2007). This concept has originally been motivated by the well-known deterioration of the visual controller with increasing distance to the observed reference object and the limitations of the camera field of view. The proposed switching approach facilitates the dynamical selection of the best suited camera from the available set of a multi-camera system in the current control situation, thereby, satisfying conditions on control performance and visibility (Kühnlenz 2007). The advantage over visual servoing with zooming cameras is obvious. Instantaneous adjustments of camera parameters are provided resulting in higher dynamics of the control system. Moreover, a significantly lower complexity of sensor model and calibration is given. Additional advantages of the proposed control scheme are task-dependent switches and switches in case of sensor breakdown.

This paper investigates the stability of sensor switching visual servoing concepts and introduces an energy supervised switching concept in order to guarantee asymptotical stability. The control error is assumed defined either in image-space or Cartesian space and the manipulator dynamics are assumed to be known exactly. Starting with an ideal and perfectly calibrated camera system, the assumptions are increasingly relaxed. It is shown that (local) asymptotical stability of switching

visual servoing with coarsely calibrated cameras is not achievable for arbitrary switching. Therefore, switching conditions based on multiple Lyapunov functions are defined in order to reduce the energy of the total system. The switching concept is applied to a visual servoing task using a switching condition based on a performance band evaluating the current control error variance. Thereby, switching cameras the error variance is kept in a small bounded region and nearly constant over the whole operating distance range.

The remainder of the paper is organized as follows: In Section 2 the switching visual servoing approaches are defined; Section 3 discusses the stability under various assumptions; simulation results are shown in Section 4; the switching concept is applied to a visual servoing task using a performance related switching condition in Section 5; conclusions are given in Section 6.

2 SENSOR SWITCHING VISUAL SERVOING

This section introduces a novel visual servoing concept with switchable cameras. In the following, conventional approaches to image-based and position-based visual servoing are recalled in brief. Based on these fundamentals, the switching control scheme is defined and several switching conditions are discussed. The section concludes with a short discussion.

2.1 Conventional Image- and Position-Based Visual Servoing

Most fundamental visual servoing concepts are image-based and position-based visual servoing, which basically differ in the definition of the control error. While the former uses a representation in image-space, the control error of the latter is defined in Cartesian space. Even though both control schemes merely differ in curvature of space and singular configurations, and from a control perspective essentially the same methods can be applied, this classification scheme has been widely accepted till to date. The basic structures are shown in the block diagrams in Figure 1 and Figure 2, respectively. In both cases, a controller computes torque inputs to a manipulator dynamics which responds with the current system state in joint coordinates. Evaluating the forward kinematics, the current joint angle configuration results in a current end-effector pose and, thus, in a current pose of the camera which is considered mounted on the end-effector (eye-in-hand).

In image-based visual servoing, the camera in the current pose responds with a current projection $s = h_i(q)$ of the feature points of an observed object from Cartesian space into image-space. The

controller compares these projections with desired projections computing a set torque input to the robot dynamics in combination with a joint-level controller. This control-law can be written

$$\tau = J_i(q, s, Z)^T K e_i(q) + K_v \dot{q} + g(q), \quad (1)$$

with τ the commanded torque vector, symmetric positive-definite gain matrices K and K_v , control error $e_i(q) = s^d - s(q)$ with current and desired feature point positions s and s^d , respectively, joint angle vector q , gravitational forces g , and the differential velocity mapping from joint-space to image-space J_i , i.e. the image-Jacobian according to (Kelly et al. 2000).

Taking the manipulator dynamics into account

$$M(q)\ddot{q} + C(q, \dot{q})\dot{q} + g(q) = \tau, \quad (2)$$

with symmetric positive-definite inertia matrix M , Coriolis and centripetal torques $C\dot{q}$, the closed-loop system dynamics in terms of the state vector $[q^T \dot{q}^T]^T$ can be written

$$\begin{aligned} \frac{d}{dt} \begin{bmatrix} q \\ \dot{q} \end{bmatrix} &= \begin{bmatrix} \dot{q} \\ M^{-1}[J_i^T K e_i(q) - K_v \dot{q} - C\dot{q}] \end{bmatrix}, \\ s &= h_i(q). \end{aligned} \quad (3)$$

Using the forward kinematics, the system responds with a current pose vector of the end-effector $W(q) = [X \ Y \ Z \ \phi \ \theta \ \psi]^T$.

In position-based visual servoing, an object model is used in order to compute the current camera pose $\bar{W} = h_t(q)$ from the current feature point projections. The controller compares the current camera pose with a desired camera pose which in combination with the joint-level controller can be written

$$\tau = J_t(q)^T K e_t(q) - K_v \dot{q} + g(q), \quad (4)$$

with the control error $e_t(q) = \bar{W}^d - \bar{W}(q)$ defined in Cartesian space, current end-effector pose $\bar{W} = [X \ Y \ Z \ \phi_X \ \phi_Y \ \phi_Z]^T$ with respect to the observed object, where $\phi_{(\cdot)}$ denotes a rotation around the respective axis (\cdot), the desired pose \bar{W}^d , and the differential mapping J_t from joint-space to Cartesian task space, i.e. the “task” Jacobian according to, e.g. (Deng et al. 2002).

Similarly to Eq. (3) the closed loop dynamics can be written

$$\begin{aligned} \frac{d}{dt} \begin{bmatrix} q \\ \dot{q} \end{bmatrix} &= \begin{bmatrix} \dot{q} \\ M^{-1}[J_t^T K e_t - K_v \dot{q} - C \dot{q}] \end{bmatrix}, \\ \bar{W} &= h_t(q), \end{aligned} \quad (5)$$

Based on the fundamental concepts of image- and position-based visual servoing in the following section a sensor switching visual servoing scheme is introduced.

2.2 Sensor Switching Visual Servoing

In this section, the conventional visual servoing concepts are extended by introducing a switchable camera in the feedback loop. Technically, this may, e.g., be realized by several different cameras mounted on the robot end-effector. The controller is designed as a switching controller selecting a current control scheme corresponding to the selected camera, which is written

$$\tau = J_{i,\sigma}^T K e_i + K_v \dot{q} + g, \quad J_{i,\sigma} \in \{J_{i,1}, \dots, J_{i,k}\} = \mathcal{J}_i, \quad (6)$$

for the image-based case with the sets $\{\mathcal{J}_{i,p} : p \in \mathcal{P}\}$ of respective Jacobians and an index set \mathcal{P} , and a piecewise constant function of time (*switching signal*) $\sigma : [0, \infty) \rightarrow \mathcal{P}$. A current camera is dynamically selected from a set $h_{i,\sigma} \in \{h_{i,1}, \dots, h_{i,k}\} = \mathcal{H}_i$ yielding a switched measurement equation

$$s = h_{i,\sigma}. \quad (7)$$

For the position-based (task space) controller the task space Jacobian does not switch. However, the sensor model h_t resolving the camera pose \bar{W} from the image space feature vector switches such that

$$\bar{W} = h_{t,\sigma}, \quad (8)$$

with $h_{t,\sigma} \in \{h_{t,1}, \dots, h_{t,k}\} = \mathcal{H}_t$.

The closed loop dynamics for the image-based architecture can, thus, be written

$$\begin{aligned} \frac{d}{dt} \begin{bmatrix} q \\ \dot{q} \end{bmatrix} &= \begin{bmatrix} \dot{q} \\ M^{-1}[J_{i,\sigma}^T K e_i - K_v \dot{q} - C \dot{q}] \end{bmatrix} = f_{i,\sigma}, \\ s &= h_{i,\sigma}, \end{aligned} \tag{9}$$

and for the position-based case

$$\begin{aligned} \frac{d}{dt} \begin{bmatrix} q \\ \dot{q} \end{bmatrix} &= \begin{bmatrix} \dot{q} \\ M^{-1}[J_t^T K e_t - K_v \dot{q} - C \dot{q}] \end{bmatrix} = f_{t,\sigma}, \\ \bar{W} &= h_{t,\sigma}, \end{aligned} \tag{10}$$

in the following represented by vector fields $f_{i,\sigma}$ and $f_{t,\sigma}$. Note that e_t is dependent on \bar{W} . Ideally e_t does not change during a switch. However, if modeling errors in \bar{W} are present then e_t also changes during a switch as perturbations add to \bar{W} which are potentially different from one another. Therefore, we write $f_{t,\sigma}$ switched dependent on the switching sequence σ . The switching signal σ might depend on t and/or $[q^T \ \dot{q}^T]^T$ or on an external input. The switching concept, thus, consists in a dynamical selection of a current tuple $\langle f_{(\cdot),\sigma}, h_{(\cdot),\sigma} \rangle$.

Also performance- and task-related issues can be considered in order to formulate a switching condition on σ (Kühnlenz 2007). Performance issues may, e.g., consider image plane limitations and tracking performance. A straightforward switching condition may switch to a different camera if feature points are about to leave the visible field of view with a side-condition of providing maximum control performance, e.g. a minimum tracking error variance or maximum sensitivity of the controller. Vice versa, if the control performance exceeds a predefined threshold then a different camera is selected under the condition of providing maximum performance while keeping all feature points in view. Of course, other issues may also be considered, e.g. if the camera currently used has to be assigned otherwise or is simply malfunctioning.

The following sections are concerned with stability investigations under various assumptions on modeling accuracy of sensor and object models.

3 STABILITY OF SENSOR SWITCHING VISUAL SERVOING

The control concept proposed in this paper switches sensor and controller within the same class of visual servoing schemes. The switching schemes are assumed to switch between visual servoing subsystems which are stable. However, it is a well known fact that a switched system composed of subsystems which are stable can be unstable. This section discusses stability based on common and multiple Lyapunov functions of switched systems. In the first part, ideal object and camera models and perfectly calibrated cameras are assumed. In the second part, these strong assumptions are relaxed and stability of the switching approach with parameter perturbations is discussed. It is noted that asymptotical stability of the proposed switching control scheme cannot be guaranteed for arbitrary switching. In order to overcome this drawback, conditions on the switching sequence evaluating the total energy of the system are introduced which assure asymptotic stability. Therefore, in the third part, an extension to switched system visual servoing is proposed introducing an energy supervised switching scheme based on multiple Lyapunov functions.

In the following section, some fundamental issues on switched system stability are recalled in brief.

3.1 Switched System Stability

A switched system can be defined as a hybrid dynamical system consisting of a family of continuous-time subsystems and a rule that orchestrates the switching between them (Liberzon 2003). Mathematically, a switched system can be described by a differential equation of the form

$$\dot{x} = f_{\sigma}(x), \tag{11}$$

with a family of vector fields f and a switching signal σ . It is assumed that the state does not jump at switching instants, the time intervals between two switches are non-zero and all subsystems are (asymptotically) stable.

Various tools exist in order to guarantee asymptotical stability of switched systems, e.g. c.f. (Branicky et al. 1994; Brockett 1993; Liberzon and Morse 1999; Liberzon 2003; Branicky 1997; Branicky 1998). Common approaches are based on Lyapunov theory using common or multiple Lyapunov

functions in order to assure a global decrease of the total energy of the system. If the family of systems $\dot{x} = f_p(x)$, $p \in \mathcal{P}$ has a common Lyapunov function V such that $\nabla V(x)f_p(x) < 0 \forall x \neq 0, p \in \mathcal{P}$ then the switched system (11) is asymptotically stable for any switching signal σ .

Otherwise, asymptotical stability can be guaranteed using multiple Lyapunov functions. As each subsystem is assumed asymptotically stable there exists a family of Lyapunov functions $\{V_p : p \in \mathcal{P}\}$ such that the value of V_p decreases on each time interval where the p -th subsystem is active. If for every p the value of V_p at the end of each such interval exceeds the value at the end of the next interval on which this subsystem is active then the switched system is asymptotically stable. This can be written

$$V_p(t_3^p) - V_p(t_1^p) < 0, \quad (12)$$

with t_1^p and t_3^p denote two time instances at the ends of two consecutive time intervals, where system p is active. For switching between two systems p and q $V_p(t_3)$ can be expressed by

$$V_p(t_3) = V_p(t_1) + (V_q(t_1) - V_p(t_1)) + \int_{t_1}^{t_2} \frac{\partial V_q}{\partial q \partial \dot{q}} f_p dt + (V_p(t_2) - V_q(t_2)) + \int_{t_2}^{t_3} \frac{\partial V_p}{\partial q \partial \dot{q}} f_q dt, \quad (13)$$

and

$$\frac{\partial V_{p,q}}{\partial q \partial \dot{q}} f_{p,q} = \dot{V}_{p,q}. \quad (14)$$

Another possibility is to ensure that the switching signal “waits” long enough at each time instance such that a global energy decrease is achieved (Liberzon 2003). A number $\tau_d > 0$ can be introduced and the class of admissible switching signals can be restricted to signals with the property that the interval between any two consecutive switching times is no smaller than τ_d . However, this approach is limited to switching between systems with equal equilibria.

In the next section stability of idealized sensor switching visual servoing is discussed using common Lyapunov functions.

3.2 Ideal Sensor Switching Visual Servoing

In this section, ideal camera and object models as well as perfectly calibrated cameras are assumed. Under these assumptions, asymptotical stability of the proposed sensor switching visual servoing system is proven for arbitrary switching using a common Lyapunov function in a straightforward manner.

Conventional image- and position-based visual servoing with robot dynamics have been proven (locally) asymptotically stable based on Lyapunov's direct method (Kelly et al. 2000). Thus, the proposed switched system can be assumed to be composed of subsystems which are asymptotically stable. These subsystems only differ in camera, camera model, and controller which are assumed to correspond perfectly to one another, i.e. no parameter perturbations are present.

The Lyapunov functions of image- and position-based visual servoing can be written

$$V_i(e_i(q), \dot{q}) = \frac{1}{2} \dot{q}^T M \dot{q} + \frac{1}{2} e_i(q)^T K e_i(q), \quad (15)$$

and

$$V_t(e_t(q), \dot{q}) = \frac{1}{2} \dot{q}^T M \dot{q} + \frac{1}{2} e_t(q)^T K e_t(q), \quad (16)$$

with current and desired joint configuration q and q^d , respectively, control errors $e_{(\cdot)}$, and symmetric positive-definite matrices M and K . The derivatives yield

$$\dot{V}_i = \dot{V}_t = -\dot{q}^T K_v \dot{q}. \quad (17)$$

As K_v is by design positive-definite \dot{V}_i as well as \dot{V}_t are negative-semidefinite. Therefore, it can be concluded that $[q^T \dot{q}^T] = [q^d \ 0^T]^T$ is a stable equilibrium. And as the set $\Omega = \{[q^T \dot{q}^T]^T : \dot{V} = 0\}$ only contains the trivial trajectory $J_{(\cdot)}^T K_p e_{(\cdot)} = 0$ applying Krasovskii-LaSalle's theorem the system is (locally) asymptotically stable (Kelly et al. 2000).

It is now assumed that the proposed switched visual servoing system switches between such systems of one class. Considering the position-based switched system, it can be noted that the pose estimations $h_{t,p}$ and $h_{t,q}$ of the p -th and q -th subsystems based on the camera and object models yield the same result under the assumption that modeling errors do not exist. In consequence, the control errors $e_{t,p}$ and $e_{t,q}$ are equal. Thus, the Lyapunov functions of both subsystems are equal

$$V_{t,p} = V_{t,q} = V_{t,c}, \quad (18)$$

and $V_{t,c}$ is a common Lyapunov function.

The switched position-based visual servoing system is, thus, (locally) asymptotically stable for arbitrary switching under the assumption of perfect camera and object models.

Considering now the switched image-based visual servoing system, it can be noted that the control error $e_{i,\sigma}$ in image-space is dependent on the current camera. In consequence, the Lyapunov functions of the p -th and q -th subsystem are different and a common Lyapunov function cannot be defined this way. However, evaluating the Lie-bracket yields $[f_{i,p}, f_{i,q}] = 0$. This is straight forward as due to the dynamically selected tuple $\langle J_{i,\sigma}, h_{i,\sigma} \rangle$ of corresponding Jacobian and camera it the vector fields $f_{i,p}$ and $f_{i,q}$ before and after a switch are equal. Thus, it can be stated that a common Lyapunov function exists for both subsystems.

The switched image-based visual servoing system is, thus, (locally) asymptotically stable for arbitrary switching under the assumption of perfect camera and object models.

In this section, it has been shown that the camera switching visual servoing concepts are (locally) asymptotically stable for arbitrary switching under the strong assumption of ideal modeling conditions. In the next section, these assumptions are relaxed allowing for modeling errors in the subsystems.

3.3 Sensor Switching Visual Servoing with Modeling Errors

In the previous section, it has been assumed that camera and object models are perfectly known. In this section, robust stability of sensor switching visual servoing is discussed considering modeling errors. First, the robustness of conventional visual servoing is briefly discussed based on (Deng et al. 2002). Afterwards, asymptotical stability of the switched visual servoing system with constraints on the switching sequence is discussed using multiple Lyapunov functions.

In the image-based case, target model and camera calibration errors are introduced affecting the desired feature vector s^d and the Jacobian J_i , respectively. As the former only affects steady-state accuracy rather than closed-loop stability, it is focused on the effect of camera calibration errors on system stability through the Jacobian. The closed-loop dynamics for image-based visual servoing with modeling errors can be written (Deng et al. 2002)

$$\frac{d}{dt} \begin{bmatrix} \tilde{q} \\ \dot{q} \end{bmatrix} = \begin{bmatrix} -\dot{q} \\ M^{-1}[\hat{J}_i^T K \tilde{e}_i - K_v \dot{q} - C \dot{q}] \end{bmatrix} = f'_i, \quad (19)$$

with erroneous Jacobian \hat{J} (calibration errors), erroneous control error $\tilde{e}_i = s^{d'} - s = h(q^{d'}) - s(q)$ with erroneous desired feature vector $s^{d'}$ (target model errors), corresponding joint configuration

$q^{d'}$, and $\tilde{q} = q^{d'} - q$.

The origin $[\tilde{q}^T \dot{q}^T]^T = 0^T$ is the isolated equilibrium of the system. Applying Lyapunov's first method analogously to Section 3.2, the closed-loop dynamics (19) can be shown to be asymptotically stable, however, locally around $[\tilde{q}^T \dot{q}^T]^T$ (Deng et al. 2002).

For the switched image-based visual servoing system $f'_{i,\sigma}$ where (19) is modified substituting $\hat{J}_i = \hat{J}_{i,\sigma}$ and $s^{d'} = s_{\sigma}^{d'}$, the general case is assumed where the modeling errors of all subsystems can be different. Then the trivial case of equal vector fields $f_{i,p}$ and $f'_{i,q}$ of the p -th and q -th subsystems before and after a switch is only an isolated case. In general, it can be assumed that the vector fields of all subsystems are in fact different. Then, $f'_{i,p}$ and $f'_{i,q}$ do not commute as in general $[f'_{i,p}, f'_{i,q}] \neq 0$. Thus, the existence of a common Lyapunov function cannot be established this way.

Therefore, different (multiple) Lyapunov functions are assumed for each of the subsystems

$$V'_{i,p}(\tilde{q}, \dot{q}) = \frac{1}{2}\dot{q}^T M \dot{q} + \frac{1}{2}\tilde{e}_{i,p}^T K \tilde{e}_{i,p}. \quad (20)$$

In the position-based case, both, the camera calibration and the target modeling errors, affect the relative pose estimation and, therefore, the closed-loop stability. It is assumed that the error is multiplicative such that $\bar{W}' = \Lambda \bar{W}$ with diagonal matrix Λ with positive elements $1 \pm \epsilon$, $0 \leq \epsilon < 1$, which is not a function of q . Then, the closed-loop dynamics then yield (Deng et al. 2002)

$$\frac{d}{dt} \begin{bmatrix} \tilde{q} \\ \dot{q} \end{bmatrix} = \begin{bmatrix} -\dot{q} \\ M^{-1}[J_t^T K \tilde{e}_t - K_v \dot{q} - C \dot{q}] \end{bmatrix} = f'_t, \quad (21)$$

where $\tilde{e}_t = \bar{W}^d - \Lambda \bar{W}$. Applying Lyapunov's first method, this system can be shown to be asymptotically stable around the origin $[\tilde{q}^T \dot{q}^T]^T = [0 \ 0]^T$.

For the switched position-based visual servoing system $f'_{t,\sigma}$ where (21) is modified substituting J_t by $J_{t,\sigma}$ and $\tilde{e}_t = \tilde{e}_{t,\sigma} = \bar{W}^d - \Lambda_{\sigma} \bar{W}$ the general case is assumed where the Λ_{σ} of each subsystem are different. Then the Lyapunov functions

$$V'_{i,p}(\tilde{e}_t, \dot{q}) = \frac{1}{2}\dot{q}^T M \dot{q} + \frac{1}{2}\tilde{e}_{t,p}^T K \tilde{e}_{t,p}, \quad (22)$$

are different and cannot be utilized for establishing a common Lyapunov function.

In both cases, multiple Lyapunov functions exist due to modeling errors. Several possibilities

exist in order to guarantee asymptotical stability of the switched system using multiple Lyapunov functions.

Looking at the Lyapunov functions of sensor switched visual servoing with parameter perturbations, it is obvious that for different perturbations the subsystems differ in equilibria and gains of the control errors. Due to this fact the dwell-time approach cannot be applied in order to assure asymptotical stability of the switched systems. Analysis of the system properties shows: i) for systems with weak damping (decreasing oscillations present) a switching sequence can be found rendering the switched system unstable; ii) allowing arbitrary switching the switched system is at best stable; iii) asymptotic stability can be achieved by constrained switching (switching conditions) assuring a global energy decrease, however, resulting in the time interval between switches approaching infinity and, thus, in a finite number of switches. The following considerations are discussed for the position-based case, but analogously apply to the image-based case.

3.3.1 An unstable case

Switching between subsystems with different equilibria can render the total system unstable. Figure 3 schematically visualizes such an unstable case of a switched system comprising two subsystems with weak damping showing isopotential levels of their respective Lyapunov functions. For reasons of simplicity consider a switching sequence, which switches between the subsystems if the current potential energy reaches a local maximum opposite to the equilibrium of the inactive subsystem. As the kinetic energy terms $\frac{1}{2}\dot{q}^T M \dot{q}$ of all subsystems are equal, the time instances of the local maxima of the potential energy terms are equal. Thus, the corresponding isopotential level of the second system after a switch is always larger than in the previous time interval where this system was active. This results in a global increase of the total energy of the switched system. Figure 4 shows the corresponding simulation results for a simple switched visual servoing task. From these examples, it is obvious, that for weakly damped subsystems a switching sequence can always be found rendering the switched visual servoing system with parameter perturbations unstable.

3.3.2 Stability

In order to show that a switched visual servoing system with parameter perturbations allowing arbitrary switching is at best stable, but not asymptotically stable, consider two position-based visual servoing subsystems with different parameter perturbations $\Lambda_p \neq \Lambda_q$. The equilibria of the

subsystems are $[q_p^{d'T} \dot{q}^T]^T = [q(\Lambda_p^{-1}\bar{W}^d) \ 0]^T$ and $[q_q^{d'T} \dot{q}^T]^T = [q(\Lambda_q^{-1}\bar{W}^d) \ 0]^T$ with $\Lambda_p^{-1}\bar{W}^d \neq \Lambda_q^{-1}\bar{W}^d$. Consider now that both subsystems are assumed asymptotically stable. The state of the switched system will approach one of the equilibria of the subsystems if $\exists t^*$ such that $\forall t > t^* \sigma(t) = i$ as schematically depicted in Figure 5. Then, the switched system is asymptotically stable. However, allowing for arbitrary switching sequences and, thus, for infinite switches, such a t^* does not exist. It is also straight forward to see, that there exists no $\delta > 0$ for which each subsystem approaches its equilibrium $\lim_{t \rightarrow \infty} \|q^{d'} - q\| = 0$ if $\|q(0) - q^{d'}\| < \delta$. The state of the first subsystem will always be drawn away from its equilibrium if the second subsystem is active. Thus, the switched visual servoing system with parameter perturbations is not asymptotically stable. Figure 6 shows simulation results of a stable switching scheme where it is switched between two asymptotically stable subsystems with parameter perturbations.

However, in order to achieve asymptotical stability of the switched system, switching conditions can be applied which assure a global decrease of the total energy of the switched system. These switching conditions restrict the set of switching signals to admissible sequences. Such a switched system approach with constrained switching is discussed in the following section.

3.4 Assuring Asymptotical Stability by Energy Supervision

In the previous section, it has been discussed that sensor switched visual servoing with parameter perturbations is not asymptotically stable allowing arbitrary switching. In this section, a generic extension to switched system visual servoing is proposed introducing an energy supervised switching scheme in order to overcome this drawback. Thereby, the admissible set of switching sequences is restricted and asymptotical stability is guaranteed. Energy supervision has been used in order to guarantee passivity, e.g. for networked control systems (Hannaford and Ryu 2002; Hirche 2005). To the best of the authors' knowledge this concept has not yet been applied to switched visual servoing systems.

The approach consists in an observation of the total energy of the switched visual servoing system evaluating the multiple Lyapunov functions. Observing the progression of the total energy in each time interval where, e.g., the p -th subsystem is active, a switching condition is defined assuring a global decrease of the total energy of the switched system over time. A straightforward solution is, e.g., to allow switches from the p -th to the q -th subsystem not before the current value of the

total energy of the p -th subsystem falls below a threshold dynamically defined by the last value of the total energy in the previous interval where p was active. Therefore, we apply the condition for asymptotic stability (12) and restrict the set of admissible switching sequences to

$$\mathcal{S} = \{\sigma \in \Sigma : V_p(t_{i+3}^p) - V_p(t_{i+1}^p) < 0 \forall p \in \mathcal{P}\}, \quad (23)$$

where t_{i+1}^p and t_{i+3}^p denote two time instances at the ends of two consecutive time intervals, where system p is active, which is visualized in Figure 7. The schematic concept of energy supervised camera switching visual servoing is depicted in Figure 8.

Another advantage of such an energy supervised switching concept is its large independence of system parameters as only the system state is evaluated which is directly observable.

3.5 Discussion

In this section a camera switching visual servoing concept has been introduced which has been shown to be (locally) asymptotically stable for arbitrary switching under the assumption of perfect target and camera models. It has been shown that the switched system with parameter perturbations is not asymptotically stable for arbitrary switching. Therefore, a constrained switching scheme based on a restriction of the set of admissible switching sequences by energy observation has been introduced which assures asymptotic stability.

So far, modeling errors have been assumed small with respect to the regions of convergence of the subsystems. Thus, it has been implicitly assumed that all the equilibria of the subsystems lie within the intersection of all neighborhoods of these equilibria where asymptotical stability is guaranteed. In case of larger modeling errors, it is apparent that the region of convergence of one subsystem can be exceeded during the activity of another subsystem. Larger modeling errors, thus, can cause the system to reside in local minima of the controller, e.g. which are present in the overobserved case of image-based visual servoing, where a nonempty nullspace exists. Beside local minima, also singularities can be present which can be hit after a switch. Further investigations would be desirable accounting for the regions of convergence of the subsystems. However, to our knowledge these regions have never been firmly established yet. So, these aspects remain an open problem for camera switching visual servoing.

There are other not considered shortcomings which, however, are caused by common stability

and performance problems of the underlying visual servoing schemes. Examples are certain effects of large physical motions in image-based visual servoing which have been discussed in (Chaumette 1998) and the field of view problem in position-based visual servoing. These drawbacks, however, do not limit the basic idea presented in this paper and can be overcome with a variety of state-of-the-art tools.

4 SIMULATION STUDIES ON SENSOR SWITCHING VISUAL SERVOING

In the previous section, switching visual servoing concepts allowing for dynamical sensor selection have been introduced and discussed. In this section, the proposed approach is exemplarily applied to a standard visual servoing task with a large general motion of the end-effector and two dynamically selectable cameras. Three cases are studied. Two simulation runs are conducted with different switching sequences resulting in a large and a small activation time period of the subsystem with camera 1, respectively. A third simulation run is conducted adding an energy supervised condition to the latter scenario with the smaller activation time. In the following, the simulation layout is described and the obtained results are discussed.

4.1 Simulation Layout

Exemplarily, an image-based architecture is chosen and the control task consists in a desired pose of the camera system right in front of a target object with its optical axis orthogonal to the object plane. The initial pose is set such that the camera system is in a sideview pose with respect of the target with rotational offsets around the optical and yaw axes. The camera pose trajectory, thus, results in a large general motion as shown in Figure 9. The camera system consists of two cameras mounted on the end-effector with coaxial optical axes. As the end-effector moves along the trajectory the active camera is dynamically switched by a periodical switching sequence. Two sequences are simulated with different time periods $\tau_{1,a} = 200ms$, $\tau_{1,b} = 1080ms$ where the first camera is active. The resulting image-space and Cartesian space errors as well as the propagation of the values of the multiple Lyapunov functions are shown in Figure 10 for a switching sequence with equal activation times of both cameras of 0.1s. For reasons of clarity of the switching effects,

manipulator dynamics are modeled as a basic mass-damper system with six degrees-of-freedom and joint-space and task-space are assumed equal. A camera framerate of $30ms$ and a conversion time delay of $30ms$ are assumed. Pixel sizes are $0.00001m \times 0.00001m$ and a quantization of the feature point position estimation of $0.000001m$ are chosen. The gains are $K_p = 400$ and $K_v = 400$ and the manipulator inertia matrix is $M = 0.5\text{diag}(1kg, 1kg, 1kg, 1kgm^2, 1kgm^2, 1kgm^2)$. For better clarity of the diagrams no sensor noise is assumed. The target object has edge lengths of $0.5m$. The initial camera pose is $\bar{W}_{t=0s} = [1m \ 0m \ -0.2m \ 0rad \ -1.3rad \ 0.5rad]^T$ and the final pose is $[\bar{W}_{t=\infty} = [0m \ 0m \ -1m \ 0rad \ 0rad \ 0rad]^T$. The focal-length of camera 1 is $\lambda_1 = 10mm$ and the one of camera 2 is $\lambda_2 = 20mm$. Small errors of the object model and the focal-length of 10% are set for the subsystem with camera 1. The camera model of camera 1 assumes a focal-length of $\lambda_1 = 11mm$ and an image center point displacement such that the target object in the final pose has a pose offset of $2.5cm$ in all Cartesian directions. The model of camera 2 is ideal.

The third simulation scenario adds an energy supervised switching condition to the switching sequence with $\tau_{1,a}$ such that switches to camera 2 are only permitted when the current value of the Lyapunov function of the subsystem with camera 1 is below its last value in the previous time interval where this subsystem was active.

4.2 Discussion of Results

Figures 10 to 13 show the results of the simulation studies for the three considered scenarios. Figure 10 exemplarily shows the progression of the control errors in image-space and Cartesian space and of the multiple Lyapunov functions. It can be noted that the values of the multiple Lyapunov functions form a globally decreasing sequence. It can also be noted that in the initial transient phase the values of the Lyapunov function of one subsystem at the ends of the respective activation time periods do also form a decreasing sequence. This switched system is apparently stable.

A notable difference between the three simulation runs with different switching sequences can be noted in the steady-state behaviors. Figures 11 to 13 show the progression of the average image error and the Lyapunov functions for the cases defined in the previous section. It can be noted that after some time step the total energy of the switched system without energy supervision settles between some energy values. The switching sequence with the shorter active time period $\tau_{1,a}$ of subsystem 1 results in a higher average energy value of the system (see Figure 11) than the switching sequence with active time period $\tau_{1,b}$ (see Figure 12). In consequence, the control error is significantly lower

for the second switching sequence. Yet, in both cases the switched system is not capable of reducing the error any further and results in oscillations around the equilibrium. By these switching schemes only stability is achieved.

In contrast, the energy supervised switching scheme continues to reduce the total energy and, thus, the control error of the system towards subpixel accuracy. Thus, it has been successfully demonstrated that the proposed constrained switching scheme renders the switched system asymptotically stable.

In summary, the simulation studies successfully demonstrated stability of the proposed switching visual servoing concepts. The approach of energy supervision provides a tool to guarantee asymptotical stability and, thus, a notable improvement of the control performance of sensor switching visual servoing.

5 APPLICATION TO PERFORMANCE DEPENDENT CAMERA SWITCHING

Visual servoing suffers from a distance-dependent pose error and pose error variance. Using conventional visual servoing techniques this drawback cannot be overcome due to the trade-off between the field of view and the sensitivity of the vision system. A minimum field of view has to be guaranteed in order to be able to observe a reference object at the nearest distance. However, this constraint results in a weaker sensitivity at larger distances to the observed object and, thus, in increased pose errors and variances.

In this section the proposed switching approach is applied to a standard visual servoing task and a performance related switching condition is used in order to cope with the distance dependent performance of the controller. The advantages of the proposed switching scheme over zooming cameras have already been discussed in Section 1.

A desired trajectory of the camera consisting of a translation along and a rotation around the optical axis is defined which is shown in Figure 15d. A set \mathcal{H}_i of three sensors with focal-lengths of $\lambda \in \{10\text{mm}, 20\text{mm}, 40\text{mm}\}$ and corresponding controllers $\mathcal{J}_{i,j}$ based on the visual Jacobian are defined. The switching condition is defined by a variance band of $\sigma_z^0 = 6.25 \cdot 10^{-6}\text{m}^2$ of the controlled camera pose in direction of the optical axis and a side-condition to provide a maximum field of view. Thus, each time the variance band is exceeded the next camera and controller from the

sets are selected which provide a maximum possible field of view without violating the performance criterion.

Figure 15 shows the results for the trajectory following task. The standard deviation (Figure 15b) is kept within a small band reaching from approx. 0.004m to 0.008m. For comparison the standard deviations for the unswitched task are shown in Figure 16 for each of the cameras from the set. The standard deviations of the switching strategy reach approximately the values of the unswitched task for the corresponding cameras and active intervals, but the overall variability is significantly lower. The spikes, which can be noted in the standard deviation diagram are caused by the switches. After a switch the desired feature value changes with the sensor, but the current value is still taken from the previous sensor due to time delay. Thus, the control error at this time instance is very high. This effect can be reduced by mapping the previous value of the feature vector to the image space of the new sensor or by definition of a narrower variance band as switching condition.

The effectiveness of the proposed switching strategy has been shown successfully. Additional contributions of this approach are a guaranteed control performance shown by means of a bounded pose error variance and a low variability of the performance over the whole operating range. The strategy contributes to ensure high control performance over large operating ranges and is suited for combination with many of the visual servoing approaches from known literature.

6 CONCLUSIONS

In this paper, stability of camera switching visual servoing has been discussed. It has been shown, that the switched visual servoing system is (locally) asymptotically stable for ideal target and camera models and arbitrary switching establishing a common Lyapunov function. If modeling errors or parameter perturbations exist, the switched system has been shown to be at best stable, but not asymptotically stable for arbitrary switching due to different equilibria of the subsystems caused by parameter perturbations.

In order to overcome this drawback, an energy supervised approach has been introduced. This approach restricts the set of admissible switching sequences and thereby guarantees a global decrease of the total energy of the switched system rendering the switched system asymptotically stable.

This approach is restricted by sensor quantization, which establishes a lower bound to the control error. However, this restriction can be overcome using state-of-the-art feature extraction and

estimation approaches providing subpixel accuracy. The effectiveness of energy supervised switching has been demonstrated in simulations resulting in a significantly reduced control error compared to unsupervised switching. In this work energy supervision has been used for the first time in visual servoing. The discussed advantages and promising results suggest a similar beneficial impact on other switched system visual servoing concepts.

From the novel concept of sensor switching several new challenges arise which have been pointed out and have not been considered yet. The issue of potentially different regions of convergence of the subsystems has been discussed, which may still cause the switched system to become unstable if the intersections of these regions are too small or actually empty. As these regions have not been firmly established yet, this remains an open problem in switched system visual servoing. The discussed issue of local minima and singularities possibly being hit during a switch is another challenge and subject to future work.

ACKNOWLEDGEMENTS

The authors would like to thank Prof. Sandra Hirche for inspiring discussions. This work has been supported in part by the German Research Foundation (DFG) grant BU 1043/5 and the DFG excellence initiative research cluster *Cognition for Technical Systems – CoTeSys*, see also www.cotesys.org.

References

- Branicki, M., V. Borkar, and S. Mitter (1994). A unified framework for hybrid control. In *Proc. of the IEEE Conf. on Decision and Control (CDC)*.
- Branicky, M. (1997). Stability of hybrid systems: State of the art. In *Proc. of the IEEE Conference on Decision and Control (CDC)*, pp. 120–125.
- Branicky, M. (1998). Multiple lyapunov functions and other analysis tools for switched and hybrid systems. *IEEE Transactions on Automatic Control* 43, 475–482.
- Brockett, R. W. (1993). Hybrid models for motion control systems. In H. L. Trentelman and J. C. Willems (Eds.), *Essays in Control*, pp. 29–53. Boston, MA, USA: Birkhäuser.

- Chaumette, F. (1998). Potential problems of stability and convergence in image-based and position-based visual servoing. *The Confluence of Vision and Control, Lecture Notes in Control and Information Sciences 237*, 66–78.
- Chaumette, F., K. Hashimoto, E. Malis, and P. Matinet (2004). Tutorial on advanced visual servoing, tutorial notes. In *Tutorial TTP₄ at IEEE/RSJ IROS*.
- Corke, P. (1994). Visual control of robot manipulators - a review. In K. Hashimoto (Ed.), *Visual Servoing*, pp. 1–32. World Scientific.
- Corke, P. and S. Hutchinson (2001). A new partitioned approach to image-based visual servoing. *IEEE Transactions on Robotics and Automation* 17(4), 507–515.
- Deguchi, K. (1998). Optimal motion control for image-based visual servoing by decoupling translation and rotation. In *Proc. of the IEEE/RSJ Int. Conf. on Intelligent Robots and Systems (IROS)*, pp. 705–711.
- Deng, L., F. Janabi-Sharifi, and W. Wilson (2002). Stability and robustness of visual servoing methods. In *Proc. of the IEEE Int. Conf. on Robotics and Automation (ICRA)*.
- Deng, L., F. Janabi-Sharifi, and W. Wilson (2005). Hybrid motion control and planing strategies for visual servoing. *IEEE Transactions on Industrial Electronics*, 1024–1040.
- Espiau, B., F. Chaumette, and P. Rives (1992). A new approach to visual servoing in robotics. *IEEE Transactions on Robotics and Automation* 8, 313–326.
- Feddema, J. and O. Mitchell (1989). Vision-guided servoing with feature-based trajectory generation. *IEEE Transactions on Robotics and Automation* 5, 691–700.
- Gans, N. and S. Hutchinson (2007). Stable visual servoing through hybrid switched-system control. *IEEE Transactions on Robotics and Automation* 23(3), 530–540.
- Hager, G. (1995). Calibration-free visual control using projective invariance. In *Proc. of the Int. Conf. on Computer Vision (ICCV)*, pp. 1009–1015.
- Hannaford, B. and J.-H. Ryu (2002). Time-domain passivity control of haptic interfaces. *IEEE Transactions on Robotics and Automation* 18(1), 1–10.
- Hashimoto, K. and T. Noritsugu (2000). Potential problems and switching control for visual servoing. In *Proc. of the IEEE/RSJ Int. Conf. on Intelligent Robots and Systems (IROS)*, pp. 423–428.

- Hayman, E. (2000). *The use of zoom within active vision*. Ph. D. thesis, University of Oxford.
- Hirche, S. (2005). *Haptic telepresence in packet switched communication networks*. Ph. D. thesis, Dept. of Electrical Engineering and Information Technology.
- Hosoda, K., H. Moriyama, and M. Asada (1995). Visual servoing utilizing zoom mechanism. In *Proc. of the IEEE/RAS Int. Conf. on Robotics and Automation (ICRA)*, pp. 178–183.
- Hutchinson, S., G. Hager, and P. Corke (1996). A tutorial on visual servo control. *IEEE Transactions on Robotics and Automation* 12, 651–670.
- K. Hashimoto, Ed. (1993). *Visual Control of Robots: High Performance Visual Servoing*. Hong Kong: World Scientific.
- Kelly, R., R. Carelli, O. Nasisi, B. Kuchen, and F. Reyes (2000). Stable visual servoing of camera-in-hand robotic systems. *IEEE/ASME Transactions on Mechatronics* 5(1), 39–48.
- Kragic, D. and H. I. Christensen (2002). Survey on visual servoing for manipulation. Technical Report ISRN KTH/NA/P-02/01-SE, CVAP259, Stockholms Universitet.
- Kühnlenz, K. (2007). *Aspects of Multi-Focal Vision*. Ph. D. thesis, Dept. of Electrical Engineering and Information Technology, TU München, Munich, Germany.
- Kühnlenz, K. and M. Buss (2005). Towards multi-focal visual servoing. In *Proc. of the IEEE/RSJ Int. Conf. on Intelligent Robots and Systems (IROS)*, pp. 2336–2341.
- Kühnlenz, K. and M. Buss (2007). Multi-focal visual servoing strategies. In G. Obinata and A. Dutta (Eds.), *Vision Systems: Applications*. Vienna, Austria: Advanced Robotic Systems Int.
- Liberzon, D. (2003). *Switching in Systems and Control*. New York: Birkhäuser.
- Liberzon, D. and A. Morse (1999). Basic problems in stability and design of switched systems. *IEEE Control Systems Magazine* 19(5), 59–70.
- Malis, E. (2001). Visual servoing invariant to changes in camera intrinsic parameters. In *Proc. of the Int. Conf. on Computer Vision (ICCV)*, pp. 704–709.
- Malis, E. and S. Benhimane (2003). Vision-based control with respect to planar and non-planar objects using a zooming camera. In *Proc. of the IEEE Int. Conf. on Advanced Robotics*.
- Malis, E., F. Chaumette, and S. Boudet (1999). 2-1/2d visual servoing. *IEEE Transactions on Robotics and Automation* 15, 238–250.

- Mansard, N. and F. Chaumette (2004). Tasks sequencing for visual servoing. In *Proc. of the IEEE/RSJ Int. Conf. on Intelligent Robots and Systems (IROS)*.
- Martinet, P., J. Gallice, and D. Khadraoui (1996). Vision-based control law using 3d visual features. In *Proc. WAC*, pp. 497–502.
- Papanikolopoulos, N. P., P. K. Khosla, and T. Kanade (1993). Visual tracking of a moving target by a camera monted on a robot: A combination of vision and control. *IEEE Transactions on Robotics and Automation* 9(1), 14–35.
- Weiss, L. E., A. C. Sanderson, and C. P. Neumann (1987). Dynamic sensor-based control of robots with visual feedback. *IEEE Transactions on Robotics and Automation* RA-3, 404–417.
- Wilson, W. J., C. C. W. Hulls, and G. S. Bell (1996). Relative end-effector control using Cartesian position-based visual servoing. *IEEE Transactions on Robotics and Automation* 12(5), 684–696.

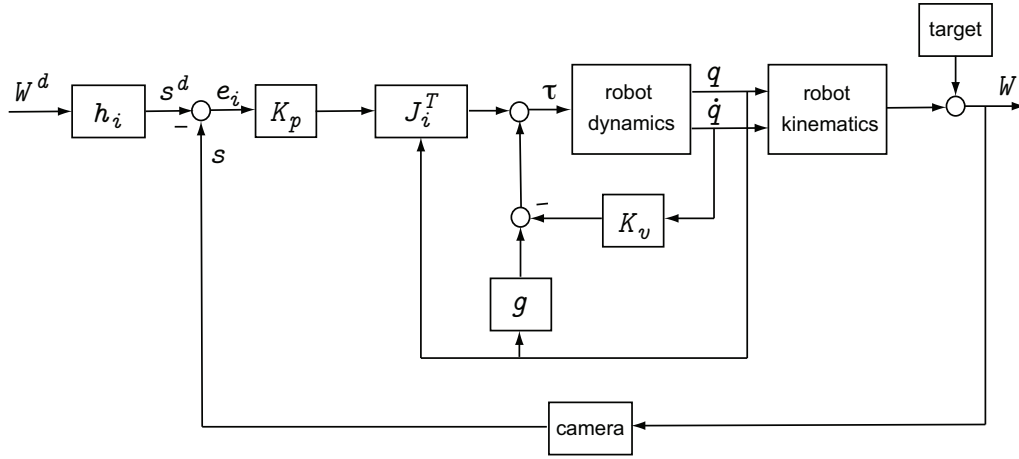


Figure 1: Conventional image-based visual servoing architecture.

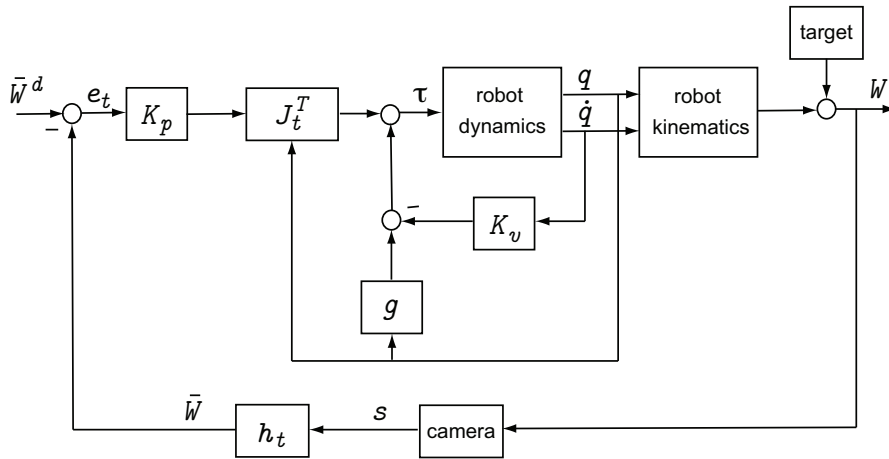


Figure 2: Conventional position-based visual servoing architecture.

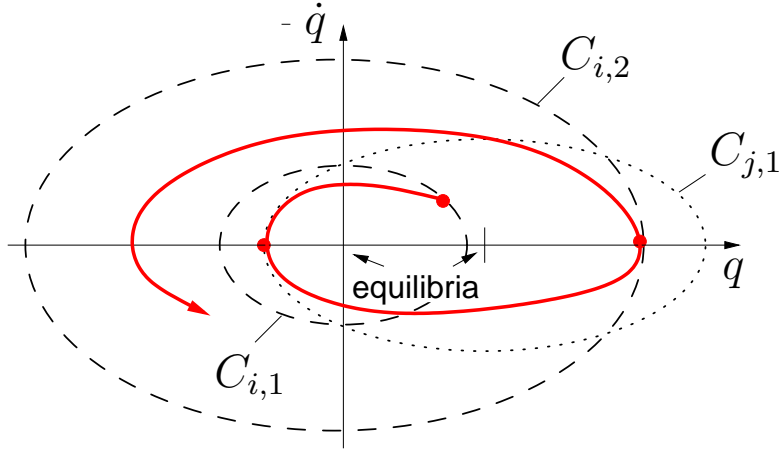


Figure 3: Switched visual servoing system with parameter perturbations; unstable switching scheme.

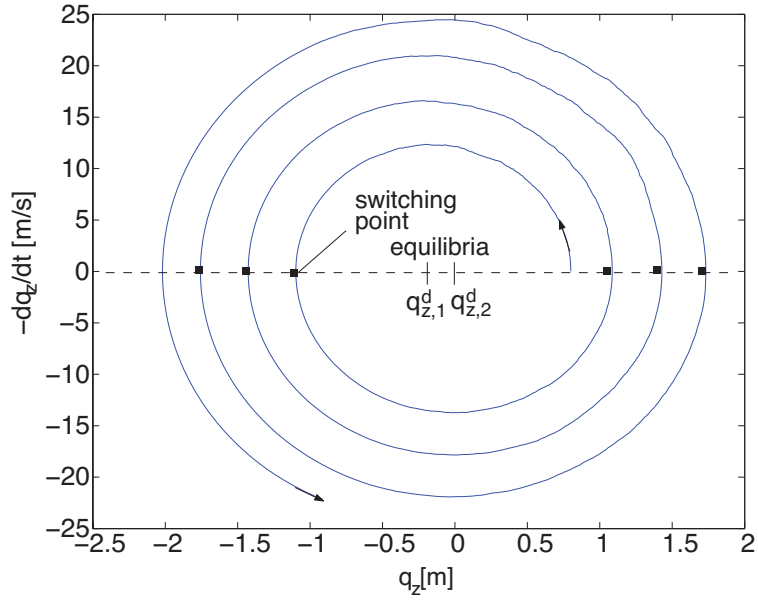


Figure 4: Simulation results; switched visual servoing system with parameter perturbations; unstable switching scheme; $\bar{W} = q$; initial position offset $q_z = 0.8m$; inertia matrix $M = 5\text{diag}(1\text{kg}, 1\text{kg}, 1\text{kg}, 1\text{kgm}^2, 1\text{kgm}^2, 1\text{kgm}^2)$, damping $K_v + C = 24\text{diag}(1\text{kgs}^{-1}, 1\text{kgs}^{-1}, 1\text{kgs}^{-1}, 1\text{kgms}^{-1}, 1\text{kgms}^{-1}, 1\text{kgms}^{-1})$, no feedback quantization, sensor noise power $\sigma_{meas}^2 = 0.00001^2\text{m}^2$, control gain $K_p = 400$.

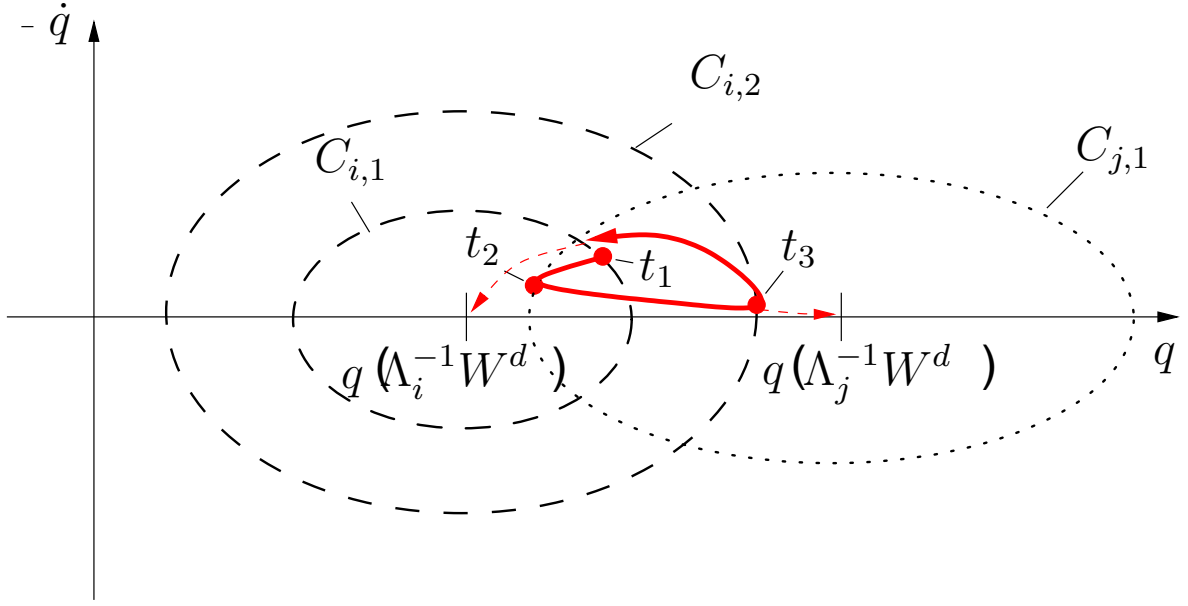


Figure 5: Switched visual servoing system with parameter perturbations; stable, but not asymptotically stable switching scheme.

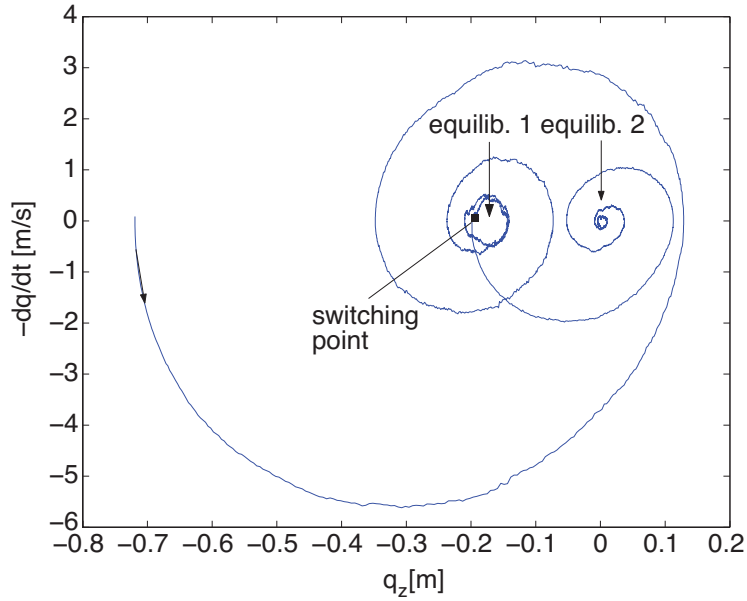


Figure 6: Simulation results; switched visual servoing system with parameter perturbations; stable, but not asymptotically stable switching scheme; $\bar{W} = q$; initial position offset $q_z = -0.7m$; inertia matrix $M = 5\text{diag}(1\text{kg}, 1\text{kg}, 1\text{kg}, 1\text{kgm}^2, 1\text{kgm}^2, 1\text{kgm}^2)$, damping $K_v + C = 1.2\text{diag}(1\text{kgs}^{-1}, 1\text{kgs}^{-1}, 1\text{kgs}^{-1}, 1\text{kgms}^{-1}, 1\text{kgms}^{-1}, 1\text{kgms}^{-1})$, no feedback quantization, sensor noise power $\sigma_{meas}^2 = 0.00001^2\text{m}^2$, control gain $K_p = 400$.

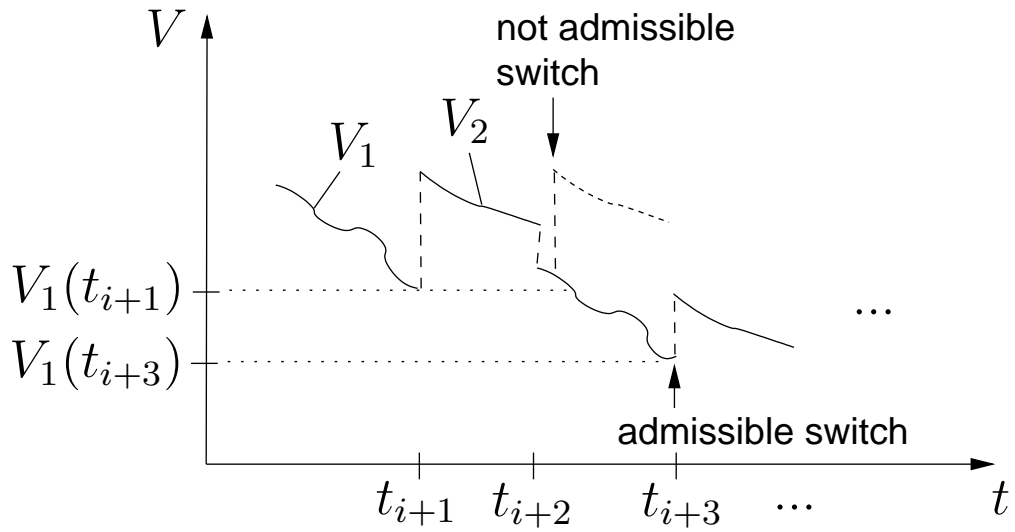


Figure 7: Restriction of the set of admissible switching sequences by energy observation assuring asymptotic stability.

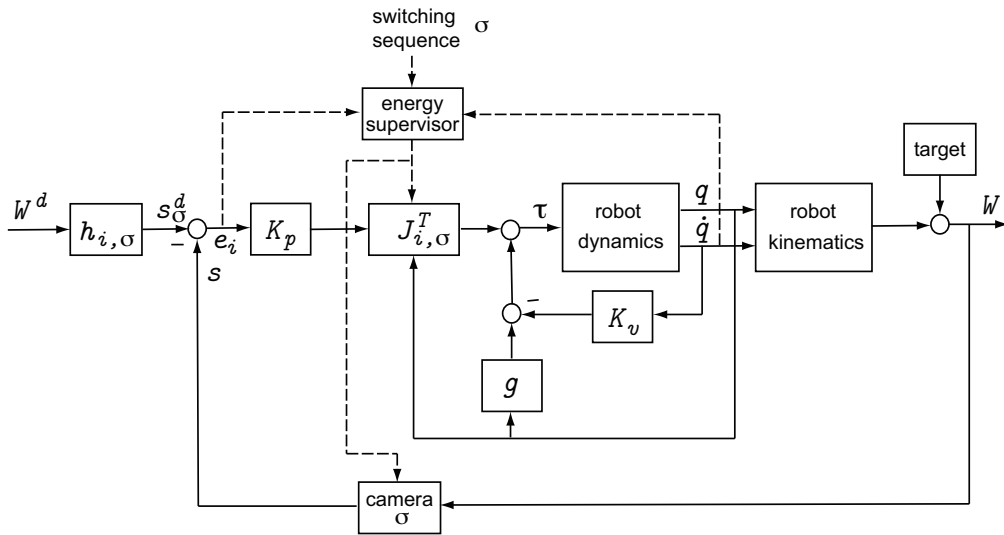


Figure 8: Energy supervised camera switching visual servoing architecture. The current total energy of the system is observed and switches are only permitted if a global energy decrease is not affected.

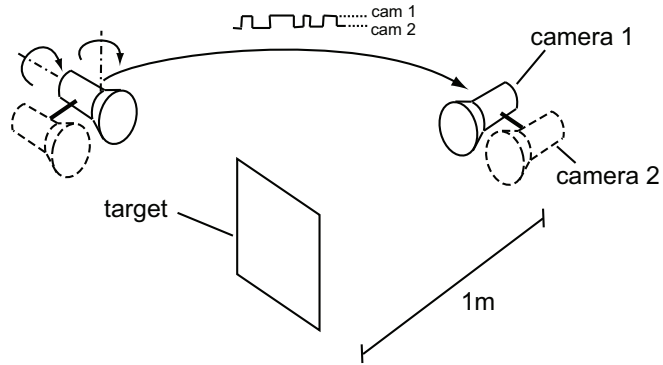


Figure 9: Simulation scenario for camera switching visual servoing.

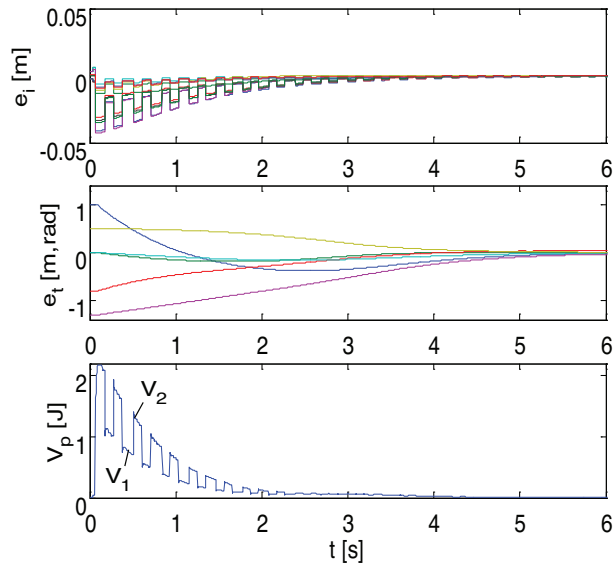


Figure 10: Exemplary results of camera switching visual servoing task; image-based architecture; control error in image-space, control error in Cartesian space, and progression of the values of the Lyapunov functions; switching time intervals of 100ms.

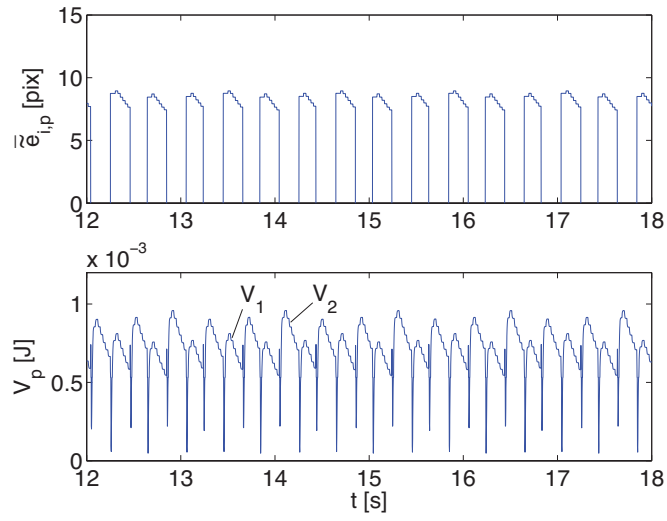


Figure 11: Results of camera switching visual servoing task; progressions of average control error and Lyapunov functions; switching period of 0.4s; time interval of subsystem 1 $\tau_{1,a} = 0.2s$.

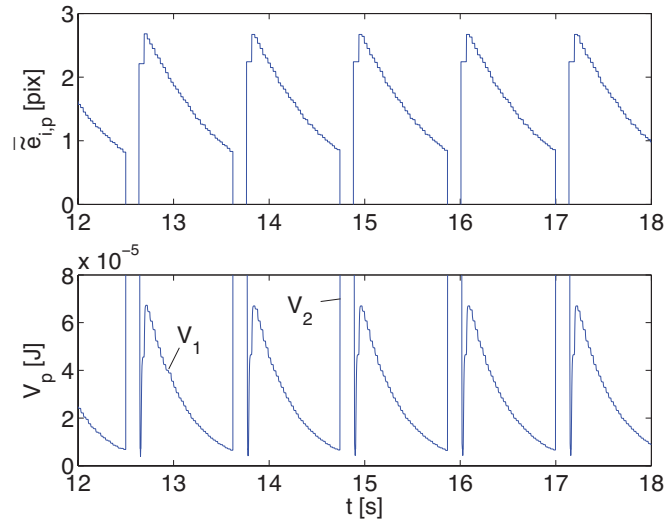


Figure 12: Results of camera switching visual servoing task; progressions of average control error and Lyapunov functions; switching period of 1.2s; time interval of subsystem 1 $\tau_{1,b} = 1.08s$.

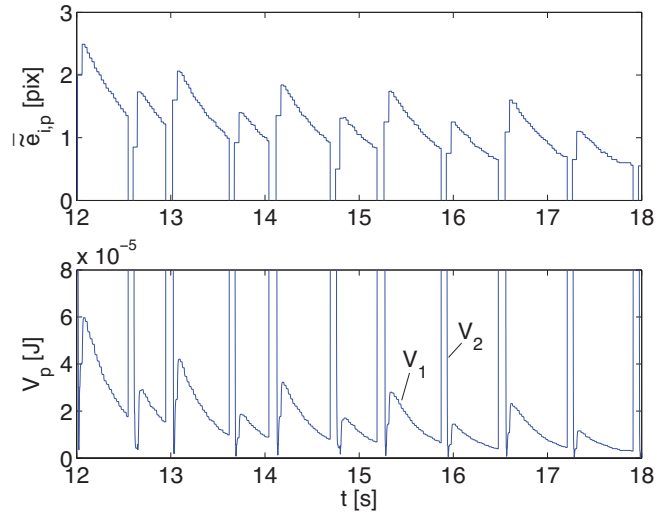


Figure 13: Results of energy supervised camera switching visual servoing task; progressions of average control error and Lyapunov functions; switching period of original switching sequence of 0.4s; original time interval of subsystem 1 $\tau_{1,a} = 0.2s$.

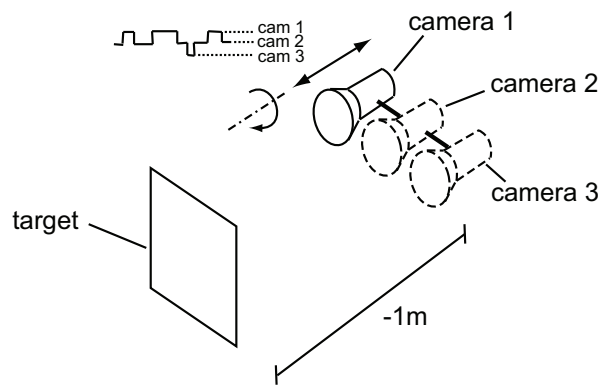


Figure 14: Visual servoing scenario with performance dependent camera switching.

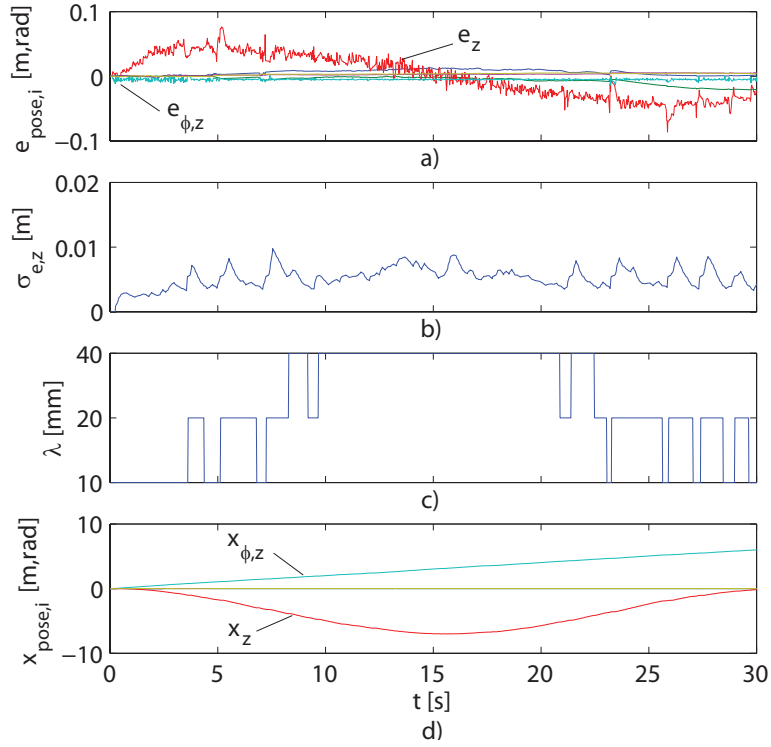


Figure 15: Visual servoing trajectory following task results with performance dependent camera switching; a) tracking errors $e_{pose,i}$, b) short-time tracking error standard deviation estimates $\sigma_{e,z}$, c) current selected focal-length λ , and d) trajectory $x_{pose,i}$ over time t (difference from initial pose); inertia matrix $M = 0.05\text{diag}(1\text{kg}, 1\text{kg}, 1\text{kg}, 1\text{kgm}^2, 1\text{kgm}^2, 1\text{kgm}^2)$, damping $K_v + C = 0.2\text{diag}(1\text{kgs}^{-1}, 1\text{kgs}^{-1}, 1\text{kgs}^{-1}, 1\text{kgms}^{-1}, 1\text{kgms}^{-1}, 1\text{kgms}^{-1})$, feedback quantization 0.00001m , sensor noise power $\sigma_{meas}^2 = 0.00001^2\text{m}^2$, control gain K_p tuned to converge system after approximately 2s.

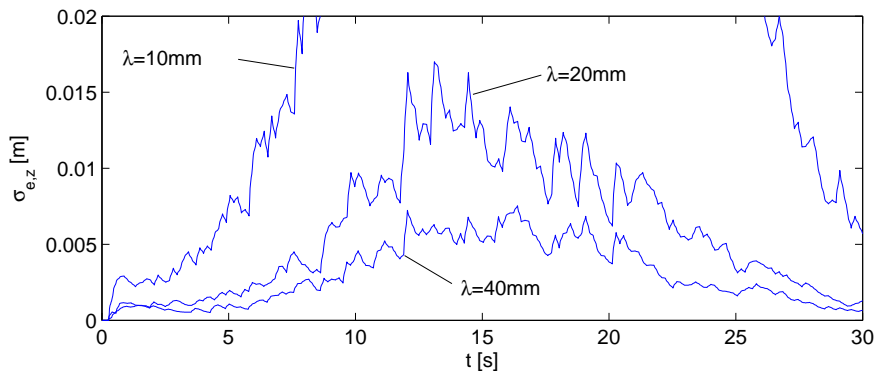


Figure 16: Short-time tracking error standard deviation estimates of unswitched single camera visual servoing task with three different focal-lengths.